

NUMERICAL MODELLING OF HIGHLY COMPLEX FLOWS

Jorge M. M. Barata^{1*}, and André R. R. Silva²

1: Aerospace Sciences Department
Engineering Faculty
University of Beira Interior
Rua Marques Avila e Bolama, 6201-001 Covilhã, Portugal
e-mail: jbarata@ubi.pt, web: <http://aeronautics.ubi.pt>

2: Aerospace Sciences Department
Engineering Faculty
University of Beira Interior
Rua Marques Avila e Bolama, 6201-001 Covilhã, Portugal
e-mail: andre@ubi.pt web: <http://aeronautics.ubi.pt>

Keywords: Numerical Errors, Modelling Errors

Abstract *This paper presents a computational study of an impinging jet through a low velocity crossflow. The purpose of this study is to quantify the relative influence of numerical and modelling sources of errors of a computational method based on the solution of the Reynolds-averaged Navier-Stokes equations and the standard “k- ϵ ” turbulence model. The accuracy of the discretization of the convection terms is quantified for first and second order numerical schemes. Additionally, the ability of the model calculations to simulate both the mean and the turbulence fields is examined and quantified using different methods. A new method of assessment of the numerical errors based on direct comparison with measurements is proposed. The new method revealed some potential to better understand the difficulties associated with the numerical prediction of complex flows, and is an interesting tool to evaluate present numerical methods more accurately.*

1. INTRODUCTION

The use of the Navier-Stokes equations to describe both laminar and turbulent flows is generally accepted. However, their analytical solution is only possible for some simplified cases, namely laminar flows. The alternative to calculate practical fluid flows relies on numerical simulation of the fundamental partial differential equations. In engineering problems the use of the Reynolds averaged Navier-Stokes equations (RANS) together with a turbulence model is widely adopted with quite success. In this case, turbulence modelling errors add to the numerical errors associated with the discretization of the partial differential equations. In spite of the computationally intensive disadvantage direct numerical solution of

the fundamental equations (DNS) is also being used [1]. A less computationally intensive approach is the large eddy simulation (LES), that divides the flow into large eddies that are resolved directly and sub grid eddies that are represented by a force, which is defined in an improvised way. All of these methods suffer from discretization and aliasing errors that are associated with the numerical method employed [2]. RANS and LES also include errors due to the turbulence and sub filter scale model, respectively.

Typically, the quantification of numerical errors by comparison with analytical solutions is only feasible for simple linear equations, for instance Laplace's and wave equation that are of limited use for complex flows due to their non-linear nature. So, the studies on optimal procedures to represent numerically the fundamental partial differential equations still continues. Additionally, to avoid the masquerading of errors due to the sub-grid and turbulence models, the quantification of the numerical errors are required and need to be kept to a small level when compared with them. Previous work has been concentrated of the analysis of accuracy and stability of the finite difference or finite element methods [4]. Those studies would like to make a comparison between the exact and the discrete solutions, but that has not been achievable. So, some interpolation is being used to extend the values of the discrete set of points to the continuum domain, which is not free from errors.

In the present work, two methods [5, 6] to determine the numerical errors were used for the test case of a turbulent impinging jet through a crossflow. A new method of quantification of numerical errors is developed in the present work that consists in the comparison with experimental direct measurements using high accuracy and precision method of Laser Doppler Velocimetry.

Next section describes the mathematical model, including the methods of accessing the accuracy of solution. Section 3 compares the three methods and discusses the results. The last section presents the main conclusions of this work.

2. MATHEMATICAL MODEL

2.1. Governing Differential Equations

The flow description of a turbulent flow involves the solution of the Navier-Stokes and continuity equations:

$$\rho \frac{DU_i}{Dt} = \rho F_i - \frac{\partial p}{\partial x_i} + \frac{\partial}{\partial x_j} \left\{ 2\mu \left(e_{ij} - \frac{1}{3} e_{ii} \delta_{ij} \right) \right\} \quad (1)$$

$$\frac{1}{\rho} \frac{D\rho}{Dt} + \frac{\partial U_i}{\partial x_i} = 0 \quad (2)$$

with

$$e_{ij} = \frac{1}{2} \left(\frac{\partial U_i}{\partial x_j} + \frac{\partial U_j}{\partial x_i} \right) \quad (3)$$

The Reynolds averaged form of these equations for steady, uniform-density isothermal three-dimensional flow may be written as

$$\rho \bar{U}_j \frac{\partial \bar{U}_i}{\partial x_j} = -\frac{\partial p}{\partial x_i} + \frac{\partial}{\partial x_j} \left(\mu \frac{\partial \bar{U}_i}{\partial x_j} - \rho \overline{u'_i u'_j} \right) \quad (4)$$

$$\rho \frac{\partial \bar{U}_i}{\partial x_i} = 0 \quad (5)$$

where the over bars represent averaged quantities.

The turbulent diffusion fluxes are estimated with the high Reynolds number version of the two-equation “ k - ε ” model:

$$\overline{u'_i u'_j} = -\nu_T \left(\frac{\partial \bar{U}_i}{\partial x_j} + \frac{\partial \bar{U}_j}{\partial x_i} \right) + \frac{2}{3} k \delta_{ij} \quad (6)$$

$$k = \frac{1}{2} \left(\overline{u'^2} + \overline{v'^2} + \overline{w'^2} \right) \quad (7)$$

where k is the turbulent kinetic energy and ν_T is the turbulent kinematic viscosity expressed by $c_\mu k^2/\varepsilon$. Since the normal stresses have an action similar to the pressure forces, the second part of Equation 6 is included in the pressure gradient term by substituting the static pressure by $p + \frac{2}{3} \rho k$.

The values for k and ε are obtained by solving the following transport equations:

$$\rho \bar{U}_j \frac{\partial k}{\partial x_j} = \frac{\partial}{\partial x_j} \left(\frac{\nu_T}{\sigma_k} \frac{\partial k}{\partial x_j} \right) - \overline{u'_i u'_j} \frac{\partial \bar{U}_i}{\partial x_j} - \varepsilon \quad (8)$$

$$\rho \bar{U}_j \frac{\partial \varepsilon}{\partial x_j} = \frac{\partial}{\partial x_j} \left(\frac{\nu_T}{\sigma_\varepsilon} \frac{\partial \varepsilon}{\partial x_j} \right) - C_1 \frac{\varepsilon}{k} \overline{u'_i u'_j} \frac{\partial \bar{U}_i}{\partial x_j} - C_2 \frac{\varepsilon^2}{k} \quad (9)$$

C_μ	C_1	C_2	σ_k	σ_ε
0.09	1.44	1.92	1.0	1.3

Table 1. Turbulence model constants

The numerical solution for turbulent flows requires the approximate solution of a set of discretized algebraic equations derived from the partial differential equations 4-5 and 8-9, that they represent. This discretization is obtained with a finite-differences/finite-volume method (e.g. [7]), which requires the integration of the transport equations in each control volume defined by a non-uniform tridimensional mesh. The governing equations are written in a similar form:

$$\frac{\partial U \phi}{\partial x} + \frac{\partial V \phi}{\partial y} + \frac{\partial W \phi}{\partial z} = \frac{\partial}{\partial x} \left(\Gamma_\phi \frac{\partial \phi}{\partial x} \right) + \frac{\partial}{\partial y} \left(\Gamma_\phi \frac{\partial \phi}{\partial y} \right) + \frac{\partial}{\partial z} \left(\Gamma_\phi \frac{\partial \phi}{\partial z} \right) + S_\phi \quad (10)$$

where ϕ represents each mean velocity component, turbulent kinetic energy or dissipation, and the transport coefficient Γ_ϕ and the source term S_ϕ take on different representations for each particular ϕ .

2.2. Numerical Methods

The numerical methods define the way to representing the values of the primitive variables in the faces of the control volumes as a function of the neighbouring values. These methods are most relevant to the stability and precision of the solution, because the use of an infinite number of points, that would allow an exact solution of the differential equations is not feasible. So, it is always necessary to verify that the solution of the discretized equations satisfies some relevant properties of the exact solution, even for coarse grids, exhibiting physical realism and a correct global balance. A method of finite differences/finite volume must maintain the conservation principles associated with the differential equations. The effect of any disturbance in some convected variable can only be propagated in the direction of the velocity; and the values of those quantities should remain within the boundary values, with no overshooting's or undershooting's.

In the present work both hybrid differencing (e.g. [8, 9]) and quadratic interpolation [7] were used. In terms of a Taylor series expansion the former gives a first order approximation, and the higher order term which is neglected is a function of $\frac{\partial^2 \phi}{\partial x^2}$ (diffusive). The latter method is second order accurate and is conservative, but satisfies only partially the transport property and does not ensure the property of the limit values. In fact, it includes always three neighbouring points in each direction, and the farthest correspond always to negative influence coefficients while the closest may be negative as well, resulting in stability problems that may result in physically unrealistic solutions [10]. Nevertheless, it is possible to use strategies that preclude this problem and take advantage of the higher order of the numerical method. In the present work, the main diagonal of the influence coefficient matrix is kept dominant by moving to the right hand term of the numerical equation the contribution of each term associated with a negative influence coefficient. This procedure eliminates the contribution of the negative coefficient while increases the value of the main diagonal of the matrix.

2.3. Boundary Conditions

The computational domain has six boundaries where dependent variables are specified: an inlet and outlet plane, a symmetry plane, and three walls at the bottom, side and top of the channel. The response of the solutions to the location of the inlet and outlet planes were investigated, and their final positions are sufficiently far away from the jet so that the influence on the computed results is negligible. At the inlet boundary uniform profiles of all dependent variables are specified from the experimental results. At the outflow boundary, the gradients of dependent variables in the axial direction are set to zero. On the symmetry plane, the normal velocity vanishes, and the normal derivate of the other variables are zero. At the solid surfaces, the wall function method described in detail by [11] is used to prescribe the boundary conditions for the velocity and turbulence quantities, assuming that the turbulence is in state of local equilibrium. The jet-exit boundary is represented by a right-angled polygon, and the mass flow rates and the momentum of the jet are matched to the experimental values. Preliminary tests used the exact shape of the jet exit by modifying the cell face areas where

the hole boundary bisected the surface area of the adjacent finite-difference control volume, so that the specified jet velocity produces correct fluxes; the velocity distribution downstream of the jet exit was relatively insensitive to the assumed shape of the hole. The jet-exit boundary conditions are also prescribed from experiments.

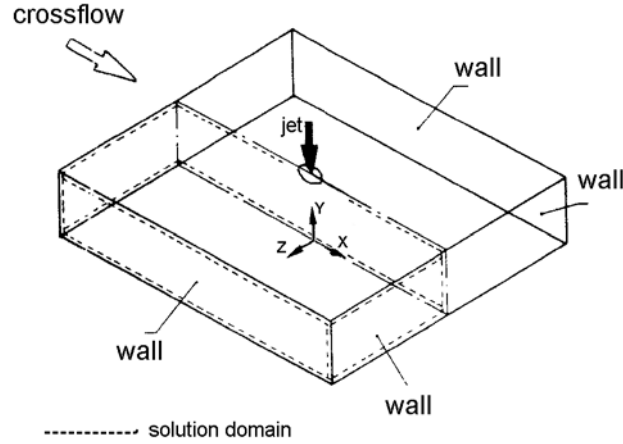


Figure 1. Solution domain.

2.4. Methods of Assessing the Accuracy of the Solution

The methods of discretization of the fundamental equations with a limited number of points introduce numerical errors that jeopardize the accuracy of the solution. Those errors need to be reduced to an acceptable level through grid refinement or more accurate numerical methods. In this subsection methods for the quantification of the numerical errors and ascertainment of the regions where they are more relevant.

The first method is due to [6] and consists in calculating the numerical diffusion error from the Taylor series expansion. For example, the representation of the convective term using central differencing is given by

$$U \frac{d\phi}{dx} = \frac{U}{2\Delta x} (\phi_E - \phi_W) \quad (11)$$

where ϕ_E and ϕ_W are the values of the dependent variable ϕ at the east neighbour E , and west neighbour W of node P , respectively.

Using the Taylor series expansion the result is the following

$$U \frac{d\phi}{dx} = \frac{U}{2\Delta x} (\phi_E - \phi_W) - \underbrace{\frac{U}{3!} \frac{d^3\phi}{dx^3} \Delta x^2 + \dots}_{\text{truncation error}} \quad (12)$$

revealing a truncation error of the order of Δx^2 . The same methodology for upwind or downwind differencing would give an even larger error of the order of Δx . According to [6] the use of the central differencing scheme to evaluate the convection term of the one-dimensional transport partial differential equation would correspond to an error which is given by the difference between equations 11 and 12:

$$T_{central} = \frac{U}{3!} \frac{d^3 \phi}{dx^3} \Delta x^2 + \dots \quad (13)$$

Accordingly, the error associated with upwind differencing would even larger:

$$T_{upwind} = \frac{U}{2!} \frac{d^2 \phi}{dx^2} \Delta x + \dots \quad (14)$$

which dominated by a diffusion like term proportional to $\frac{d^2 \phi}{dx^2}$.

The representation of the T term together with the other advection, diffusion and source terms in each transport equation of ϕ allows the identification of the zones where the numerical errors are relevant.

The second method to quantify the numerical errors interprets them as a “pseudo-diffusion” term with diffusivity in the x-direction given by

$$\Gamma_{x,f} = \frac{|U|\Delta x}{2} = \frac{|Pe|\Gamma_\phi}{2} \quad (15)$$

and identifies it as the main source of inaccuracy of the numerical methods when the velocity vector is misaligned with the grid. Ref. [5] obtained theoretically Equation 16, that quantifies the error due to the inclination of the velocity vector, and it shows that the maximum will occur for an angle $\theta = 45^\circ$ with a uniform mesh:

$$\Gamma_f = \rho \frac{|\vec{V}|\Delta x \Delta y \sin 2\theta}{4(\Delta y m^3 + \Delta x l^3)} \quad (16)$$

where l and m are the directional cosines of the velocity vector, \vec{V} is the velocity vector and Δx and Δy are the grid sizes.

If the quotient between the numerical and physical diffusion is much higher than 1 the numerical diffusion will be most relevant. The equations equivalents to equation 16 for three dimensional flows are:

$$\Gamma_{f,1} = \rho \frac{|\vec{V}|l m(l^2 + m^2)\Delta x \Delta y}{2(\Delta y m^3 + \Delta x l^3)} \quad (17)$$

$$\Gamma_{f,2} = \rho \frac{|\vec{V}|n(l^2 + m^2)}{2\left(\frac{l m^3}{\Delta x} + \frac{m n^3}{\Delta y} + (l^2 + m^2)^2 / \Delta z\right)} \quad (18)$$

$$\Gamma_{f,3} = \rho \frac{|\vec{V}|}{2\left(\frac{l m^3}{\Delta x} + \frac{m n^3}{\Delta y} + (l^2 + m^2)^2 / \Delta z\right)} \quad (19)$$

The third method was developed in the present work and revisited the common definition of accuracy as the degree of closeness of a quantity to that's true value. Since the true values are unknown high precision measured quantities using laser Doppler anemometry were used. The errors incurred in the measurements are also present but have been quantified, and may be used as the maximum error of the present method. The experimental errors have different sources. The errors due to the displacement and distortion of the measuring volume due to light refraction, to the change in the refractive index, and to non-turbulent Doppler broadening

were found to be negligibly small. The maximum error is about $10^{-4}V_j^2$ for the standard deviation and occurs in the edge of the impinging jet. The maximum error due to transit broadening in the variance of the velocity fluctuations is about $2 \times 10^{-3}V_j^2$. Largest random errors were 1.5 and 3% for the mean and turbulent values, respectively. So, the experimental values have a total error which is less than 2% for the mean values and 3,21% for fluctuating quantities.

3. RESULTS

This section presents the results obtained with the three methods described before to quantify the accuracy of the numerical errors associated with the simulation of a test case of an impinging jet through a confined crossflow for $H/D=5$ and $V_j/U_0=30$.

Figure 2 shows vertical profiles of each term in the mean vertical momentum equation together with the residual term T corresponding to the method of [6] and Equation 12. The results were obtained in different positions of the vertical plane of symmetry ($Z=0$) and hybrid differencing scheme. The results on the left column were obtained with 8,670 grid points, while those on the right correspond to a 69,360 mesh size. Both grids used expansion factors of 1.2 and 1.12, respectively, with a larger concentration of grid nodes near the axis of the impinging jet and impinging zone, and the minimum distances between points shown in Table 2.

Grid Size	$\Delta x/D$	$\Delta y/D$	$\Delta z/D$
8,670	0.16	0.035	0.05
69,360	0.065	0.015	0.015

Table 2. Minimum distances between grid nodes of the numerical meshes.

The budgets of the V-momentum equation show that for the coarser grid the term T is important near the wall ($Y=0$) and away from the impinging point ($X/D=\pm 4$). Grid refinement produces a general reduction of the T term representing the numerical errors.

Nevertheless, in regions where the diffusion term is dominant like $X/D=\pm 4$ and near the wall the errors did not decreased much. On the contrary, the budgets of the horizontal momentum equation U (that are not shown here) show a general reduction of T to values close to zero almost everywhere except near the impinging point. In this location the numerical errors did not decrease to zero with grid refinement, but the T term is much smaller than the diffusive and pressure terms. Similar conclusions can be drawn for the W-momentum equation although in this case the numerical errors also decrease substantially when the diffusive term is dominant with the pressure term.

In general, the momentum equations balances revealed that the grid refinement allows an effective reduction of the numerical errors, and the terms of the momentum equations are much larger in the region of the impinging zone where the convective and pressure terms are dominant. Away from the impinging zone, the reduction of the numerical errors

through grid refinement is not so accentuated, but nevertheless they remain quite small when compared with the convective and diffusive terms that reach the equilibrium.

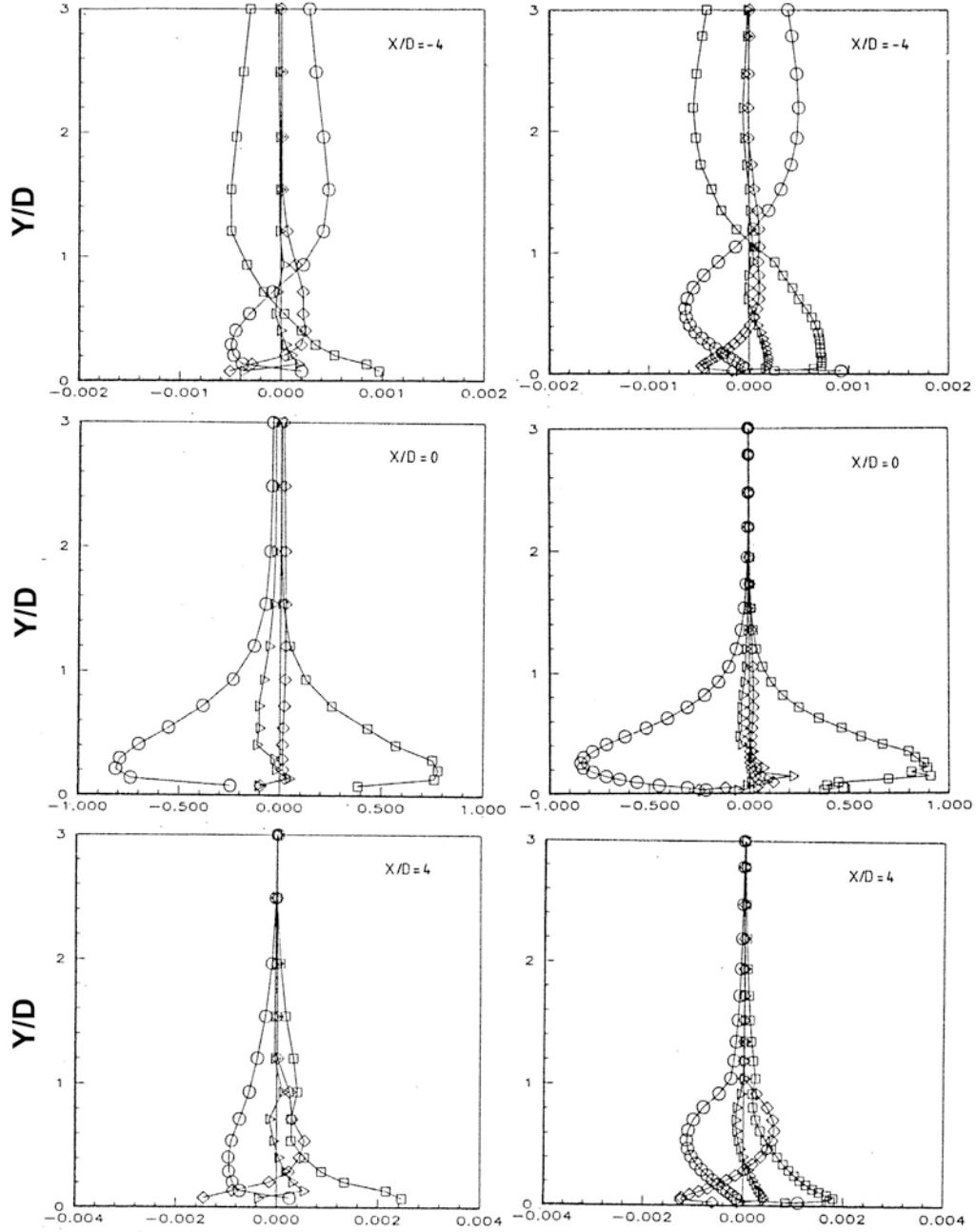


Figure 2. Vertical profiles of the V-momentum equation terms in the vertical plane of symmetry $Z=0$. O, convection; \diamond , diffusion; \square , pressure term; \triangleright , T term. (Abcissa units in $\rho V_j^2/D$). $Re_{jet}=6 \times 10^4$, $V_{jet}/U_0=30$, $H/D=5$.

Figure 3 shows isolines of the numerical diffusivity $\Gamma_{f,1}$ (Equation 17) nondimensionalized by the physical diffusivity μ_T in the vertical plane of symmetry. In this plane, $\Gamma_{f,1}$ is the only important since $\Gamma_{f,2}$ is zero, because the velocity vector is always perpendicular to the Z direction ($n=0$ in Equation 18). The largest values of $\Gamma_{numerical}/\Gamma_{physical}$ occur downstream of the impinging jet and the maximum value is reduced to one half with the finest grid. Grid refinement allows the reduction of the largest values of the numerical diffusion together with a substantial reduction of the extension of the zones where the numerical diffusivity is larger than the physical one ($\Gamma_{numerical}/\Gamma_{physical} > 1$), including the impinging jet and impinging zone where the largest gradients of the dependent variables occur.

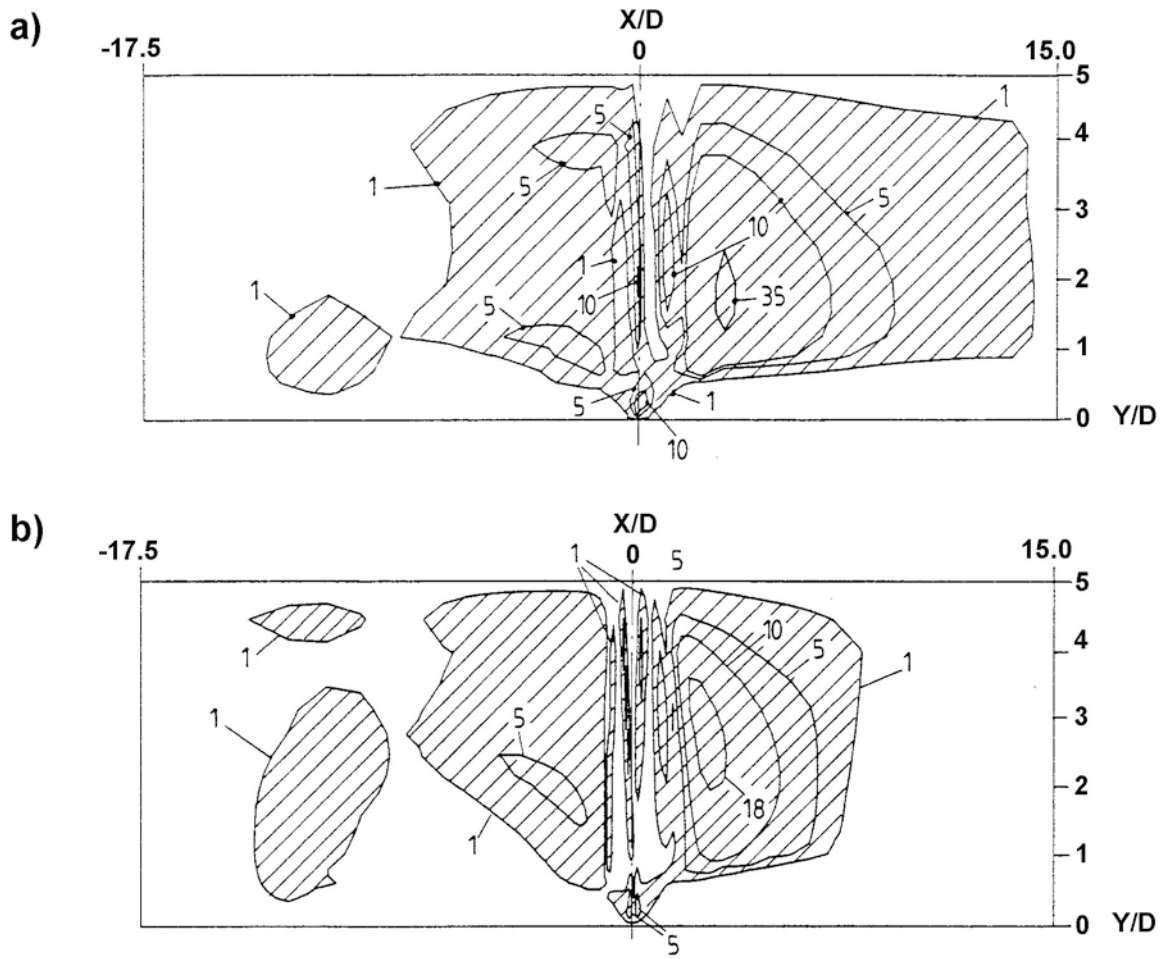


Figure 3. Isolines of the numerical diffusivity in the vertical plane of symmetry ($Z=0$): a) 8,670 mesh; b) 69,360 mesh. $Re_{jet}=6 \times 10^4$, $V_{jet}/U_0=30$, $H/D=5$.

The present study of quantification and reduction of numerical errors also includes a new method of assessment that consists in the comparison with experimental direct measurements using high accuracy and precision method of Laser Doppler Velocimetry. This method converts both the measurements and predictions to the same grid locations, and then the difference between them is analysed. The shear stress measurements are not directly compared since no direct predictions exist, and need some calculations that were performed using the numerical methodology to represent $\overline{u'v'}$ (Equation 6). Inversely, the experimental turbulent kinetic energy was obtained also indirectly from the measured normal stresses. It was assumed that $\overline{w'^2} = \frac{1}{2}(\overline{u'^2} + \overline{v'^2})$ and consequently k was calculated from $k = \frac{3}{4}(\overline{u'^2} + \overline{v'^2})$ using the measured values. The mean values of the velocity components were compared directly since they were both measured and calculated directly. The predictions using the higher order numerical method QUICK and a mesh of 8,670 points (that has been found to produce grid independent results) was used.

Figure 4 shows isolines of the difference between the measured and calculated mean horizontal velocity component in the vertical plane of symmetry ($Z = 0$). The results reveals maximum deviations from the measurements in a very small zone near the impinging point at $X/D = 0$ reaching -6% of V_{jet} which is agreement with the other methods. However, the highest values of numerical diffusivity shown in Figure 3b are not confirmed by the present method that shows a general agreement of the predictions with the measurements. Away from the impinging point, the deviations from the measurements are less than 2% of V_{jet} with an exception of a small region behind the impinging jet ($1.15 < X/D < 2.07, 3 < Y/D < 4.5$).

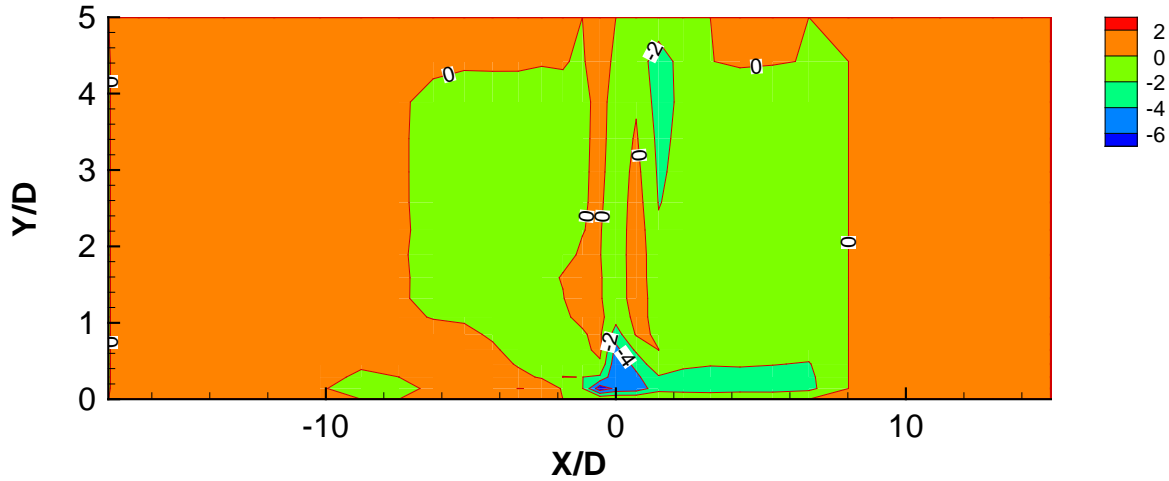


Figure 4. Isolines of numerical errors $\left(\frac{\bar{u}_{measured} - \bar{u}_{calculated}}{V_{jet}}\right) \times 10^2$ (present method), $Re_{jet} = 6 \times 10^4$, $V_{jet}/U_0 = 30$, $H/D = 5$.

When compared with the other two methods, the present method also gives different indications for the case of the mean vertical velocity component (Figure 5). The large numerical errors in the impinging zone are also observed, but away from this zone the differences between measurements and predictions are less than 5% of V_{jet} .

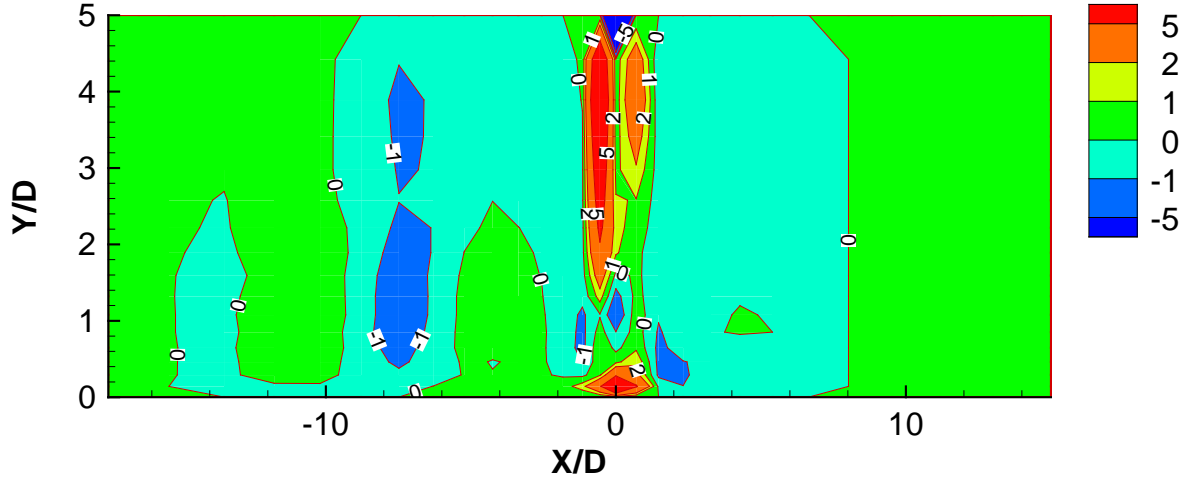


Figure 5. Isolines of numerical errors $\left(\frac{V_{measured}-V_{calculated}}{V_{jet}}\right) \times 10^2$ (present method), $Re_{jet}=6 \times 10^4$, $V_{jet}/U_0=30$, $H/D=5$.

As far as the turbulent shear stress $\overline{u'v'}$ is concerned, the maximum differences between predictions and experiments occur on either side of the impinging point, and on the shear layer surrounding the jet (Figure 6). Both the previous methods (of [5] and [6]) also identified the shear layer around the jet as regions of high numerical diffusion, but were of little help near the impinging point where high discrepancies were foreseen. This is an expected result, because near the impinging point the mean and velocities are so low, and the pressure gradient is so high that the advection term of all the equations is negligible. Nevertheless, immediately downstream of this point in each direction (with $+X$ and $-X$) relatively large differences of about 0.1% of V_{jet}^2 between measurements and predicted values are observed, that were not awaited from those methods. In fact, the turbulent kinetic energy diffusion and dissipation are habitually large as in other stagnation points, and the possible relevance of extra source terms like streamline curvature and circumferential stretching (e.g. [12, 13]) may be responsible by modelling (non-numerical) sources of errors.

Figure 7 shows measured and calculated horizontal profile of $\overline{u'v'}$ in the vertical plane of symmetry ($Z=0$) at $Y/D=0.3$ and confirms the difficulty of calculating the turbulence structure of the impinging zone. The calculated profile shows maximum values of the turbulent Reynolds stress which are three times larger than the measurements with wrong signs near the stagnation point, and are independent of numerical influences.

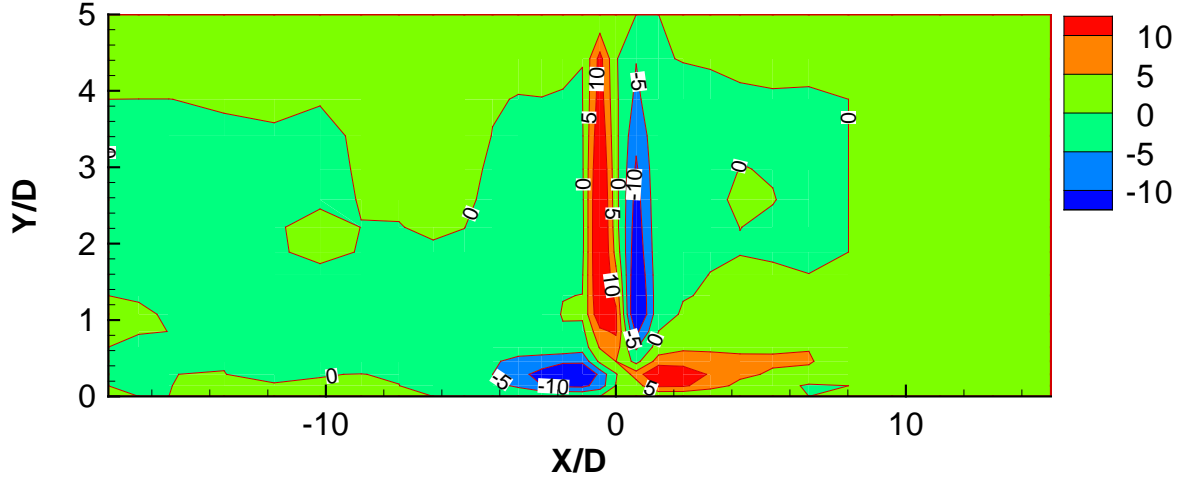


Figure 6. Isolines of numerical errors $\left(\frac{\overline{u'v'}_{measured} - \overline{u'v'}_{calculated}}{V_{jet}^2} \right) \times 10^3$ (present method), $Re_{jet}=6 \times 10^4$, $V_{jet}/U_0=30$, $H/D=5$.

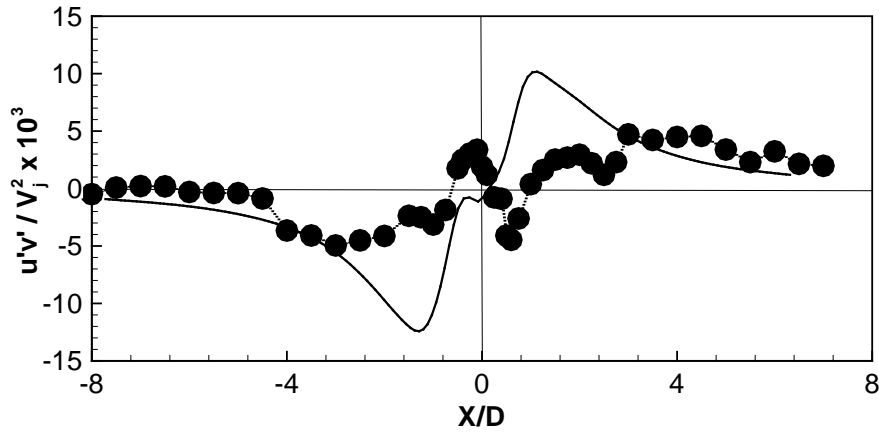


Figure 7. Horizontal profiles of the turbulent shear stress $(\overline{u'v'}/V_{jet}^2) \times 10^3$ in the vertical plane of symmetry $Z = 0$ at $Y/D = 0.3$: \bullet , experiments; —, predictions. $Re_{jet}=6 \times 10^4$, $V_{jet}/U_0=30$, $H/D=5$.

CONCLUSIONS

The numerical accuracy study of a computational model was presented for the test case of an impinging jet through a crossflow using different methods. The method of [6] concentrates on the errors associated with the numerical description of the convective term $U \frac{d\phi}{dx}$. This is a valid assumption if all the other terms are represented with second order derivatives, and no other sources of error exist. However, the present test case exhibits regions

that are dominated by very large pressure gradients, and the equilibrium with the advection term is sufficient to drive the velocity field. The method of [5] uses a different approach, but it is also focused on the advection term, and gives similar results although somewhat amplified. The present method has shown some potential to better understand the difficulties associated with numerical predictions of complex flows, and is an interesting tool to evaluate more accurate and physically available numerical tools.

REFERENCES

- [1] S. Ghosal, “An analysis of numerical errors in large-eddy simulations of turbulence”, *J. of Comp. Physics*, Vol. **125**, pp.187-206, (1996).
- [2] F. K. Chow and P. Moin, “A further study of numerical errors in large-eddy simulations”, *J. of Comput. Physics*, Vol. **184**, pp.366-380, (2003).
- [3] C. K. Chu, “Numerical methods in fluid mechanics” in *Adv. In Appl. Mechanics 18*, Academic Press, New York, pp.285-331 (1978).
- [4] P. J. Roache, *Computational Fluid Mechanics*, Hermosa Pub., Albuquerque, United States, (1972).
- [5] G. De Vahl Davis and G. D. Mallison, “An evaluation of upwind and central difference approximations by a study of recirculating flow”, *Comput. And Fluids*, Vol. **4**, pp. 29-43, (1972).
- [6] J. J. McGuirk, A. M. K. P. Taylor, “The assessment of numerical diffusion in upwind – difference calculations of turbulent recirculating flows”, in *Turbulent Shear Flows 3*. Ed. Bradbury et al, Springer-Verlag, Berlin, (1981).
- [7] B. P. Leonard, “A stable and accurate convective modelling procedure based on quadratic upstream interpolation”, *Comput. Meth. in Appl. Mech. and Engng.*, Vol. **19**, pp.59-98, (1979).
- [8] S. V. Patankar, *Numerical Heat Transfer and Fluid Flow*, Mc Graw-Hill Book Co., United States, (1980).
- [9] P. J. Roache, *Computational Fluid Dynamics*, Hermosa Pub., Albuquerque, United States, 1972.
- [10] M. A. Leschziner, “Practical evaluation of three finite-difference schemes for the computation of steady-state recirculating flows, *Comput. Meth. in Applied Mech. and Engng.*, Vol. **23**, pp. 293-312, (1980).
- [11] B. E. Launder and D. B. Spalding, “The numerical computation of turbulent flows”, *Comput. Meth. in Applied Mech. and Engng.*, Vol. **3**, pp. 269-289, (1974).
- [12] P. Bradshaw, “Effects of streamline curvature on turbulent flows”, *AGARDograph 169*, Neuilly-sur-Seine, 1980.
- [13] J.M.M. Barata, D. F. G. Durão, M. V. Heitor and J. J. McGuirk, “On the Analysis of an impinging jet in ground effects”, *Experiments in Fluids*, Vol. **15**, pp. 117-129, (1993).